IOP Conference Series: Materials Science and Engineering

PAPER • OPEN ACCESS

Oxide Growth Behaviour of Fe-Ni-Cr Alloy at High Temperature Oxidation

To cite this article: Noraziana Parimin and Esah Hamzah 2020 *IOP Conf. Ser.: Mater. Sci. Eng.* **957** 012001

IOP Conf. Series: Materials Science and Engineering **957** (2020) 012001 doi:10.1088/1757-899X/957/1/012001

Oxide Growth Behaviour of Fe-Ni-Cr Alloy at High Temperature Oxidation

Noraziana Parimin[1,*], and *Esah* Hamzah[2]

[1]School of Materials Engineering, Universiti Malaysia Perlis, 02600 Arau, Perlis Malaysia
[2]Faculty of Mechanical Engineering, Universiti Teknologi Malaysia, 81310 Skudai, Johor, Malaysia

Abstract. The isothermal oxidation test has been investigated on two types of Fe-Ni-Cr alloy, namely Fe-33Ni-19Cr and Fe-40Ni-24Cr alloys. Both alloys were undergoing an isothermal oxidation test at temperature of 500°C for 500 hours exposure time. The weight change per surface area of the oxidized samples has been recorded to calculate the oxidation kinetics of both alloys. The oxide growth behaviour of oxidized samples has been examined using scanning electron microscope (SEM) equipped with energy dispersive x-ray (EDX) spectrometer. The oxide phase formed on the sample surface has been analyzed using x-ray diffraction (XRD) technique. The results show that both alloys were followed a parabolic rate law, indicating a diffusion-controlled oxide growth mechanism. In addition, the oxidation kinetics indicating an increasing weight gain trend as the exposure time increase. Several oxide phases had formed on the oxidized surface of both alloys, consists of Cr-rich, Ti-rich, Fe-rich and spinel oxide structure. The surface morphology of both alloys demonstrated a continuous oxide scale formed on the alloy surface. Additionally, Fe-33Ni-19Cr alloy recorded a formation of Ti-rich oxide, whereas, Fe-40Ni-24Cr alloy displayed a formation of overgrown Nb-rich oxide particle which. Roles of the precipitates in oxidation mechanism give new insights into the alloy optimization.

1 Introduction

Ni-based alloy is characterized by the high phase stability of the face centre cubic austenite matrix, and are used in nuclear reactors, gas turbines, petrochemical, aerospace and heat-treating industries due to their favorable strength and excellent oxidation resistance at elevated temperature [1]. Ni-based alloy has the ability to form protective surface oxide scales at high temperatures that provides them with resistance to further high temperature oxidation [1-2]. For that reason, the oxidation behaviour of alloy has been extensively studied. Because of nickel oxide grows relatively fast, alloying element are normally added to improved its high temperature oxidation resistance, as well as mechanical properties. The element contains on the alloy is purposely added to give the topmost benefit to the alloy system in high temperature condition. Sufficient amount of each element will provide

* Corresponding author: noraziana@unimap.edu.my

protection against high temperature oxidation by forming compact, continuous slow growing oxides and thermodinamically stables compounds [3-4].

Fe-Ni-Cr alloys are a family of Ni-based alloy, which was developed for high temperature oxidizing condition. Fe-Ni-Cr alloys forms a protective surface films of Cr_2O_3, which have excellent oxidation resistance in many severe environment [5-10]. Research related to chromia forming alloy reported that Cr will enhance the formation of two oxide scale composed of Cr_2O_3 and spinel type oxide $MnCr_2O_4$. Chromia is a barrier against further oxidation due to its very low diffusion coefficients for oxygen and metals, hence offer a high oxidation resistance [8]. The study of oxidation related research on these alloys has been carried out by many researcher [1-21].

Fe-33Ni-19Cr and Fe-40Ni-24Cr alloys are usually used in power generation and thermal processing application. In these applications, the alloys are often subjected to the repeated thermal cyclic, which results a temperature gradient on heating and cooling, that affect the material properties. Therefore, microstructural stability and oxidation resistance behavior for related applications become a high priority [2]. Both alloys have higher Cr content, which are 19 and 24 % of Cr, which act as the oxide forming element. These alloys were chosen in this study due to the circumstances that typically 15-25% Cr has been identify to give best oxidation protection to the component by forming a slowly growing surface oxide scale of Cr_2O_3 during high temperature service [3]. Fe content in the alloy would favour a formation of hematite phase, which have the beneficial impact on the oxide scale spallation resistance [11-13].

In addition, alloying element has been added to both alloys to enhanced the properties during service. Minor alloying element, which are Mn, Ti, Si, Al and Nb, may significantly affect the oxidation behavior of the alloy [3-4, 14]. Si and Al will precipitates as internal oxides, while Mn and Ti may incorporate into the scale, forming a stable oxide layer. Additionally, the precipitates formation were found to have obvious influences on oxidation rate, which depends on the complex function of the alloy structure. The formation of precipitates at the scale-metal interface depends on the alloying element and working conditions of the oxidized samples. The present of the precipitates may decrease the adherence of the oxide scale to the metallic structure and contributed to the preferred site for pit formation [15-18]. Therefore, in this study, the behavior and growth of oxide scale on two types of Ni-based alloys has been investigated in terms of oxidation kinetics and oxide morphology of the oxidized samples.

2 Methodology

The materials used in this study were two types of Ni-based alloy, which are Fe-33Ni-19Cr (ASTM-B-409: ASME-SB-409, UNS N08810) and Fe-40Ni-24Cr (ASTM-B-409: ASME-SB-409, UNS N08120) alloys. The chemical composition of Fe-33Ni-19Cr and Fe-40Ni-24Cr alloys has been analyzed using optical emission spectrometer (OES). The composition of both alloys has been presented in Table 1. Samples for the high temperature oxidation tests were cut using wire electrical discharge machine (EDM) to dimensions approximately 10 mm x 10 mm x 3 mm. The samples for oxidation tests were ground using silicon carbide grinding paper to P600 grit finished. The surface area of each samples has been recorded before the oxidation test. All samples were weighted on METLER AT400 analytical balance with accuracy of ± 0.1 mg, before and after the oxidation test to measure the weight change. Both alloys were isothermally oxidized at 500°C for 500 hours. The oxidized samples were characterized in terms of oxidation kinetics, oxide phase analysis and oxide surface morphology. The oxidation kinetics was calculated form the weight change of the oxidized samples over a surface area. The oxide phase was analyzed using X-ray diffraction (XRD) model SIEMENS coupled with BRUKER D5000 XRD instrument software. The oxide scale morphology was examined using scanning electron microscope (SEM) coupled with energy dispersive x-ray (EDX) analyzer model JOEL JSM-6460 LA and PHILIPS XL40.

Table 1. Chemical composition of Fe-33Ni-19Cr and Fe-40Ni-24Cr alloys in weight percent (wt. %) with balance Fe.

Alloy / Element	Ni	Cr	C	Al	Ti	Si	Mn	P	Cu	N	Nb
Fe-33Ni-19Cr	33	19	0.078	0.534	0.489	0.315	0.556	0.007	0.082	0.02	-
Fe-40Ni-24Cr	40	24	0.048	0.080	0.029	0.441	0.702	0.014	0.114	0.20	0.44

3 Results and Discussion

3.1 Oxidation Kinetics

The weight change per surface area as a function of time of Fe-33Ni-19Cr and Fe-40Ni-24Cr alloys isothermally oxidized at 500°C for 500 hours is shown in Fig. 1. The oxidation kinetics of both alloys follows similar trend with increasing weight gain, as the exposure time increase. At the beginning of the oxidation test, both alloys recorded a rapid weight gain until 100 hours exposure time. The weight gains continuously increase as the oxidation exposure increase until 500 hours. Overall, Fe-33Ni-19Cr alloy exhibited slightly lower weight gain compared to Fe-40Ni-24Cr alloy. Similar weight change trend has been recorded by other researchers on oxidation study of Fe-Ni-Cr alloy [5, 10].

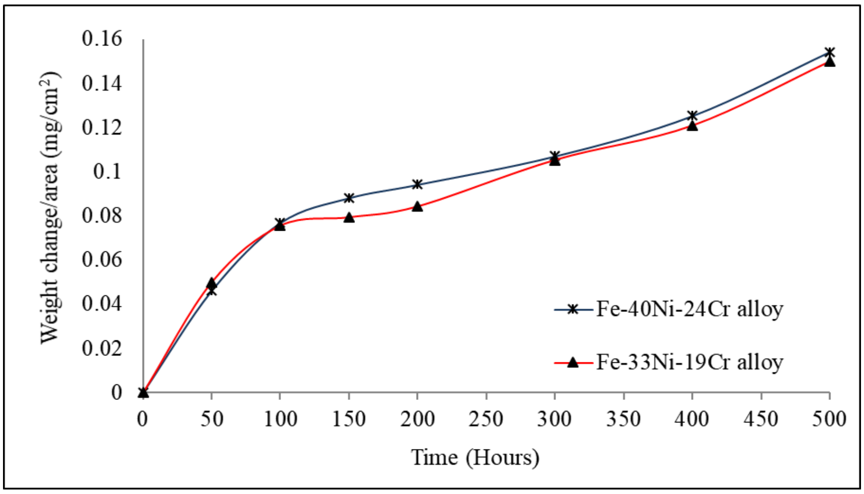

Fig. 1. Oxidation kinetics of Fe-33Ni-19Cr and Fe-40Ni-24Cr alloys at 500°C for 500 hours.

The rate law of the oxidized alloy was identified by a double log plot as shown in Fig. 2 (a). Equation (1) was used to fit the data where x is a weight change per surface area, t is a time and C is a constant. The m value indicating the rate data of the respecting curve, which value of 1, 2 and 3 for linear, parabolic and cubic oxidation, respectively. The double log plots indicate that both alloys produced good fitting results. The fitting parameter R^2 with a value approaching one denotes the increasing consistence of the data with the fitting. From the graphs, the m value for both alloys was recorded at 2.32 and 2.14 for Fe-33Ni-19Cr and

Fe-40Ni-24Cr alloys, respectively, indicating the oxidation kinetics approximately follows a parabolic rate law, m = 2. The analysis form the double log plots was confirmed that the oxidation rate law for both alloys were followed a parabolic rate law, thus lead to further identify the parabolic rate constant for both alloys. Our previous studies has found that the exposure of both alloy at others oxidizing temperatures recorded a similar parabolic rate law [15-16, 19-21]. Fig. 2 (b) shows the square of weight change as a function of time, with equation (2) was used to fit the data, where x is a weight change per surface area, t is a time, C is a constant and Kp is a parabolic rate constant. Both alloys show good fitting R^2 results. The parabolic rate constant recorded a value of 11.17 x 10^{-9} and 11.80 x 10^{-9} for Fe-33Ni-19Cr and Fe-40Ni-24Cr alloys, respectively. The parabolic rate constant for Fe-33Ni-19Cr alloy recorded a lower value, indicating a good oxidation resistance.

$$log\ x = 1/m\ log\ t + C \quad (1)$$

$$x^2 = Kp\ t + C \quad (2)$$

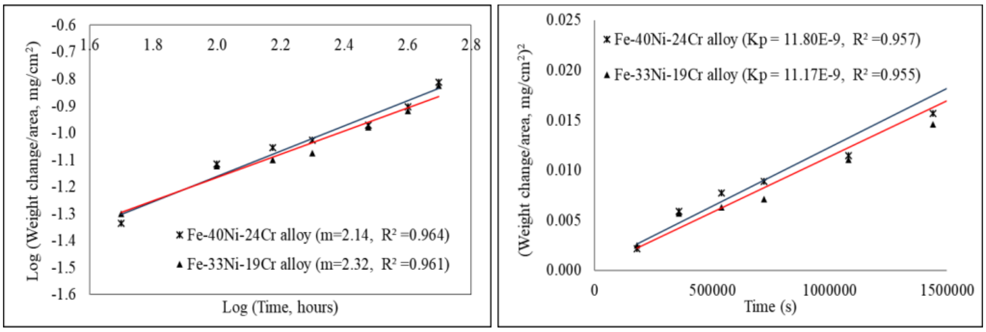

(a) (b)

Fig. 2. Weight change as a function of exposure time of Fe-33Ni-19Cr and Fe-40Ni-24Cr alloys at 500°C: (a) double log plots indicating parabolic rate law (m=2) and (b) square of weight change indicating parabolic rate constant, Kp value.

3.2 Oxide Phase Analysis

The oxide phase analysis has been done by XRD technique for both alloys. The analysis recorded that the main oxide phases formed on the alloy surface of Fe-33Ni-19Cr and Fe-40Ni-24Cr alloys composed of several oxide phases consists of Cr-rich, Fe-rich, Ti-rich and spinel oxide structures. The oxides phases are Cr-rich oxides (Cr_2O_3, $Cr_{1.3}Fe_{0.7}O_3$, $(Cr_{0.88}Ti_{0.12})_2O_3$), Fe-rich oxides ($Fe_2O_3$ and Fe_3O_4) Ti-rich oxides (TiO_2 and $(Ti_{0.97}Cr_{0.03})O_2$) and spinel oxides structure ($MnCr_2O_4$, $MnFe_2O_4$, $FeCr_2O_4$, $NiCr_2O_4$ and $NiFe_2O_4$). The presence of Cr-Ti-rich oxides, such as $(Cr_{0.88}Ti_{0.12})_2O_3$ and $(Ti_{0.97}Cr_{0.03})O_2$ oxides are believe to reduce the effect of Cr evaporation, whereby the formation of Cr evaporation lead to the development of oxide exfoliation. According to [14], the $(Cr,Ti)_2O_3$ has a lower Cr vapor pressure comparable with $LaCrO_3$ due to the same hexagonal structure in between Ti and La. Oxidized Fe-33Ni-19Cr alloy were formed several oxide phase which are Cr-rich, Fe-rich, Ti-rich and spinel oxides structure that contributes the most to the oxide formation due to rapid diffusion of these metal ion during high temperature exposure. In addition, the formation of hematite (Fe_2O_3) phase have significant impact on oxide exfoliation resistance. According to other researchers [11-13], the formation of hematite would reduce the coefficient thermal expansion (CTE) mismatch in between hematite and spinel oxide due to the similar CTE volume. On the other hand, the formation of Mn-Cr spinel oxides phase may also enhance the oxide spallation resistance due to the incorporated of Mn and Cr oxide which can lower the Cr_2O_3 activity by the formation in $MnCr_2O_4$ oxide [3-4]. While, oxidized Fe-40Ni-24Cr alloy formed similar oxide scale with Fe-33Ni-19Cr alloy, with addition of Nb-rich oxide composes of NbO_2.

3.3 Oxide Surface Morphology

Fig. 3 shows SEM image of oxide surface morphology of Fe-33Ni-19Cr alloy after exposure for 300 hours. Fig. 3 (a) shows low magnification (1000x) of SEM image, demonstrated the uniform and continuous oxide scale formed on the alloy surface with disclose of undulation surface texture of oxide layer. The undulation surface texture was originating from the grinding effect to provides a groove marks on the sample surface, which act as oxide nucleating foundation to enhance the nucleation process. The undulation surface texture indicated that thin oxide scale was formed on the alloy surface. Whereas, high magnification (10,000x) SEM image in Fig. 3 (b) displays the uniform scale-shape oxide formed on the alloy surface. The elemental EDX analysis at the matrix area (A) recorded the presence of Fe, Ni, Cr and Mn which are identified as the main elements and alloying element of the alloy. The presence of oxygen indicates the thin oxide layer developed on the alloy surface. The elemental EDX analysis suggested that area A composes of mixed oxide phases. While, EDX analysis at spot B indicates the enrichment of element O and Ti, suggested that this oxide particle composed of Ti-rich oxide. According to other researcher [14], the formation of Ti-rich oxide was said to give significant effect on oxidation protection and mitigated oxide exfoliation.

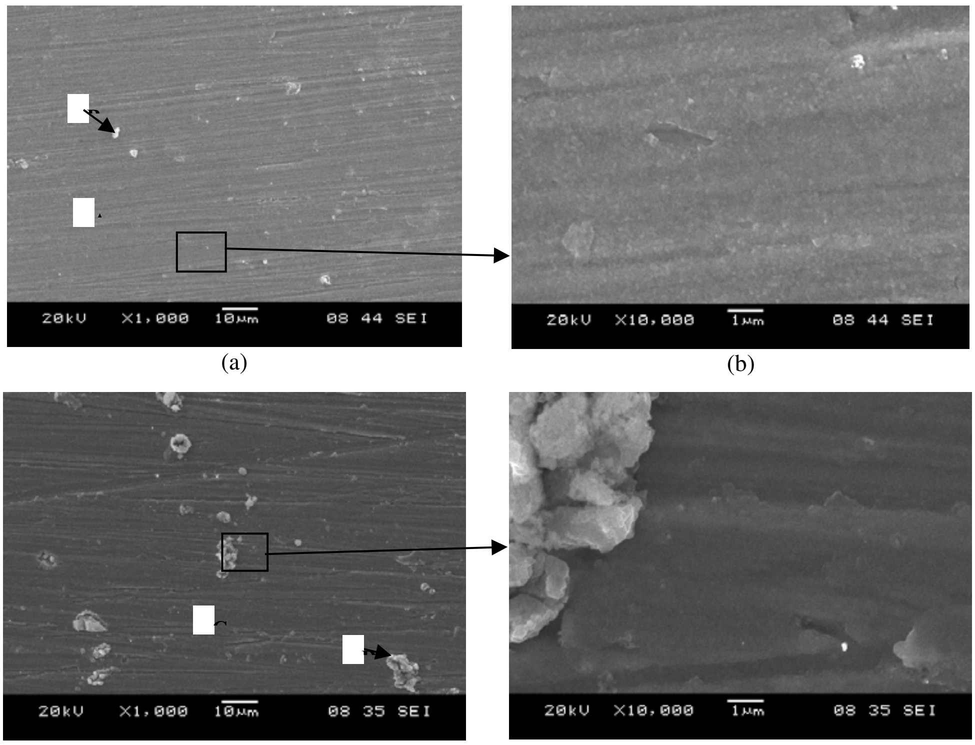

(a) (b)

(c) (d)

Fig. 3. SEM images of oxide morphology after exposure for 300 hours: (a-b) Fe-33Ni-19Cr alloy, (c-d) Fe-40Ni-24Cr alloy.

Fig. 3 (c) shows low magnification (1000x) SEM image of oxide surface morphology of Fe-40Ni-24Cr alloy after exposure for 300 hours, indicated the formation of continuous oxide layer with overgrown oxide particles distributed along the oxide surface. The Elemental EDX analysis on the area C recorded the enrichment of element Fe, Ni, Cr, Mn and O, indicating the formation of mixed oxide phases on the alloy surface. The elemental EDX analysis on the overgrown oxide particle at D recorded the enrichment of element Nb and O, suggesting the formation of Nb-rich oxide as analyzed by XRD technique. Whereas, the close-up SEM image (10,000x) in Fig. 3 (d) shows the protruding structure of overgrown Nb-rich oxide was well attached to the oxide structure. Other researcher [17-18] has recorded similar Nb-rich precipitates formed on oxidized of Ni-based alloy.

Fig. 4 (a) shows low magnification (1000x) SEM image of oxide surface morphology of Fe-33Ni-19Cr alloy after exposure for 500 hours showing a uniform and continuous oxide structure was formed on the alloy surface. The close-up SEM image (10,000x) on Fig. 4 (b) shows the similar oxide structure with indication of Ti-rich oxide particles formed at the isolated area on the alloy surface. Fig. 4 (c) shows the formation of uniform oxide structure with overgrown Nb-rich oxide particles on Fe-40Ni-24Cr alloy after exposure for 500 hours. The Nb-rich oxide particles was overgrown on the oxidized Fe-40Ni-24Cr alloy as isolated oxide particle. It is found that a crack was developed inside the overgrown oxide particles due to the effect of extensive growth of protruding oxide structure. The Nb element was added to alloy system as an alloying element to enhance the mechanical properties of the alloy. However, it is caused in the formation of Nb-rich oxide precipitates which encourages the occurrence of pitting. The presence of pitting on the oxide surface contains of Nb-rich oxide has been reported by other researcher [12], due to the massive difference in the composition between alloy matrix and precipitates. Whereas, Fig. 4 (d) shows a large area of the oxide spallation on the oxidized Fe-40Ni-24Cr alloy surface, mark as area E.

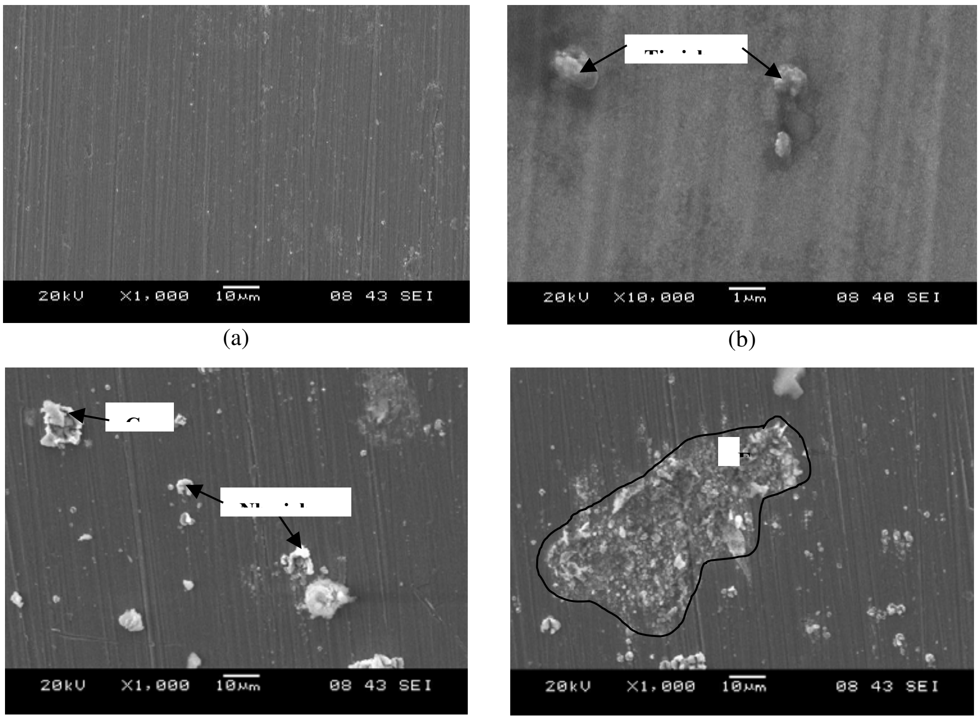

Fig. 4. SEM images of **o**xide morphology after exposure for 500 hours: (a-b) Fe-33Ni-19Cr alloy, (c-d) Fe-40Ni-24Cr alloy.

4 Summary

High temperature oxidation of Fe-33Ni-19Cr and Fe-40Ni-24Cr alloys had been study in order to investigate the oxidation kinetics, oxide phases and oxide scale behavior. The kinetics of isothermal oxidation of both alloys follow a parabolic rate law, indicating the diffusion-controlled oxide growth rate. Fe-33Ni-19Cr alloy recorded lower parabolic rate constant, therefore has good oxidation resistance. Several oxide phases were formed on the alloy surface. The oxide morphology formed on oxidized samples of both alloys are mostly uniform with mixed oxides phases detected. On the other hand, oxidized Fe-40Ni-24Cr alloy displayed a formation of overgrown Nb-rich oxide precipitates. The formation of Nb-rich oxide precipitates is significantly detrimental due to the induces of crack formation around the precipitates.

The authors would like to thank the Ministry of Education Malaysia for the research fund under the Fundamental Research Grant Scheme (FRGS) (Project Code. FRGS/1/2016/TK05/UNIMAP/02/4).

References

1. B.R. Barnard, P.K. Liaw, R.A. Buchanan, D.L. Klarstrom, Mater. Sci. & Eng.: A **527** (16-17) (2010)
2. M. Fulger, D. Ohai, M. Mihalache, M. Pantiru, V. Malinovschi, J. Nucl. Mater. **385** (2) (2009)
3. J. Zurek, D.J. Young, E. Essuman, M. Hänsel, H.J. Penkalla, L. Niewolak, W.J. Quadakkers, Mater. Sci. & Eng.: A **477** (1-2) (2008)
4. G.R. Holcomb, D.E. Alman, Scrita Mater. **54** (10) (2006)
5. S. Liu, J. Shen, X.H. Guo, L.L. Liu, Y. Niu, Corros. Sci. **135** (2018)
6. S. Swaminathan, S.M. Hong, M. Kumar, W.S. Jung, D.I. Kim, H. Singh, I.S. Choi, Surf. & Coat. Tech. **362** (2019)
7. M.S. Elbakhshwan, S.K. Gill, A.K. Rumaiz, J. Bai, S. Ghose, R.B. Rebak, L.E. Ecker, Appl. Surf. Sci. **426** (2017)
8. A. Col., V. Parry, C. Pascal, Corros. Sci. **114** (2017)
9. S. Bsat, B. Xiao, X. Huang, S. Penttila, Oxid. Met. **89** (2018)
10. B. Adam, L. Teeter, J. Mahaffey, M. Anderson, L. Arnadottir, J.D. Tucker, Oxid. Met. **90** (2018)
11. L. Tan, T.R. Allen, J,T. Busby, J. Nucl. Mater. **441** (1-3) (2013)
12. L. Tan, K. Sridharan, T.R. Allen, R.K. Nanstad, D.A. McClintock, J. Nucl. Mater. **374** (1-2) (2008)
13. L. Tan, K. Sridharan, T.R. Allen, J. Nucl. Mater. **348** (3) (2006)
14. L. Tan, X. Ren, K. Sridharan, T.R. Allen, Corros. Sci. **50** (7) (2008)
15. N. Parimin, E. Hamzah, IOP Conf. Ser.: Mater. Sci. Eng. **701** (2019) 012022
16. N. Parimin, Singh, IOP Conf. Ser.: Mater. Sci. Eng. **701** (2019) 012063
17. L. Tan, Corros. Sci. **50** (11) (2008)
18. G.S. Was, P. Ampornrat, G. Gupta, S. Teysseyre, E.A. West, T.R. Allen, K. Sridharan, J. Nucl. Mater. **371** (1-3) (2007)
19. N. Parimin, Jemahri, IOP Conf. Ser.: Mater. Sci. Eng. **701** (2019) 012062
20. N. Parimin, Z. Zulnuraini, S.A.C. Sakdun, Solid State Phenomena **280** (2018)

21. N. Parimin, E. Hamzah, A. Amrin, Solid State Phenomena **280** (2018)